
CALYREX: Cross-Attention LaYeR EXtended Transformers for System Prompt Anchoring

Li Lixing
Cornell University
Ithaca, NY 14853
11963@cornell.edu

Abstract

Modern large language models (LLMs) rely on system prompts to establish behavioral constraints and safety rules. Standard causal self-attention treats privileged instructions and untrusted user content with equal structural priority—a mismatch that leaves models vulnerable to prompt injection and instruction erosion over extended contexts. We propose **CALYREX** (Cross-Attention LaYeR EXtended transformers), which utilizes cross-attention between input and system prompt to structurally isolate and anchor the rule. A placement ablation on a 1.5B backbone identifies insertion at the final eighth of layers as optimal, confirmed by mechanistic activation analysis showing behavioral constraints are naturally concentrated there. At 8B scale, controlling for training data, backbone, and parameter budget, CALYREX yields +7.4% on instruction-following (IFEval) and +16.3% on multi-turn instruction adherence, while reducing many-shot jailbreaking attack success rate by 13%. This advantage appears to widen with model scale, consistent with larger models more effectively utilizing the dedicated routing pathway.

1 Introduction

Modern LLM deployment relies on a *system prompt* to establish behavioral constraints and safety rules, yet standard Transformers process all tokens through a uniform causal self-attention mechanism [Vaswani et al., 2017] that treats privileged instructions and untrusted user data with equal priority—a structural mismatch Wallace et al. [2024] term the Instruction Hierarchy problem.

This uniform priority yields two critical problems. First, models suffer from prompt injection, where adversarial user inputs overwrite the system prompt’s rules and successfully hijack the model’s objective [Perez and Ribeiro, 2022, Abdelnabi et al., 2023]. Second, models suffer from the gradual erosion of system instructions over extended or multi-turn sequences.

Current solutions treat this as a behavioral flaw. Techniques such as SFT, LoRA [Hu et al., 2022], preference optimization [Chen et al., 2025b], and structured delimiters [Chen et al., 2025a] teach rule-following by modifying weights, incurring an SFT distribution shift penalty that overwrites pre-trained reasoning.

We hypothesize that robust rule-following is not a behavioral problem to be solved with data, but a structural routing problem to be solved with architecture. We propose **CALYREX** (Cross-Attention LaYeR EXtended transformers), which inserts (system prompt-full input) cross-attention blocks between self-attention blocks to enforce system-prompt-following structurally. By inserting zero-initialized cross-attention blocks and training them on small general datasets on a frozen backbone, the architecture structurally preserves pre-trained reasoning while learning to route system-prompt constraints. By comparison with baseline models, we can isolate the architectural advantage from confounding variables such as dataset, backbone model and block placement locations.

Through a high-resolution ablation study on a 1.5B parameter probe, we provide a systematic characterization of where rule-adherence capacity is localized in a frozen LLM backbone—finding it concentrated in the final eighth of layers—and use this finding to identify the optimal CAL placement. Scaling this architecture to an 8B model suggests a scale-dependent trend of architectural advantage: while improvements over a parameter-matched structural baseline are modest at 1.5B, they widen at 8B on strict and extended instruction-following, multi-turn adherence, and many-shot jailbreak resistance.

Our contributions are:

1. **The CALYREX architecture:** cross-attention conditioning on the system-prompt span, inserted into a transformer to structurally enforce system-prompt priority without overwriting pre-trained semantics.
2. **Spatial locality ablation:** a systematic study across eight CAL placement strategies on a 1.5B backbone, characterizing where rule-following constraints are localized and identifying the final eighth of layers as the optimal insertion zone.
3. **Scale-dependent evaluation:** a preliminary observation (at 1.5B and 8B scale) that CALYREX’s architectural advantage over a parameter-matched structural baseline widens with model size on strict and extended instruction-following, multi-turn adherence, and many-shot jailbreak resistance, with no consistent advantage observed on strict extraction or direct-attack security benchmarks.

2 Related Work

Cross-Attention Conditioning in Multimodal Models. Flamingo [Alayrac et al., 2022] and BLIP-2 [Li et al., 2023] insert cross-attention blocks into a frozen decoder, sourcing K/V from a separate vision encoder; ControlNet [Zhang et al., 2023] conditions a frozen diffusion backbone via zero-initialized convolutional copies. CALYREX shares the zero-initialized insertion topology but sources K/V from a *privileged span within the same sequence*—adapting multimodal conditioning to the intra-sequence privilege-separation problem.

Prompt Injection and Behavioral Alignment. Prompt injection [Perez and Ribeiro, 2022, Abdelnabi et al., 2023] exploits the uniform treatment of all input tokens. SecAlign [Chen et al., 2025b] and StruQ [Chen et al., 2025a] defend behaviorally via preference optimization and structured delimiters; the Instruction Hierarchy framework [Wallace et al., 2024] shows behavioral fine-tuning substantially improves adherence. CALYREX complements these approaches by enforcing system-prompt priority *architecturally*, making structural routing the primary mechanism rather than a weight-encoded policy.

Mechanistic Interpretability of Rule Representations. Representation engineering [Zou et al., 2023] and feed-forward vocabulary promotion [Geva et al., 2022] both show that behavioral constraints are localized in late-stage layers. This spatial bottleneck motivates our placement ablation and the use of the final eighth of layers as the optimal insertion zone, confirmed with mechanistic activation analysis in Section 4.3.

3 Architecture

Let \mathcal{M} be a pre-trained causal decoder language model. At any given layer l , the model maintains a hidden state (residual stream) $\mathbf{X}^{(l)} \in \mathbb{R}^{B \times T \times d}$, where B is the batch size, T is the sequence length, and d is the hidden dimension.

Every sequence passed to the model is assumed to contain a *system prompt*: a privileged instruction span defined by an opening and closing delimiter. For any sequence b in a batch, we denote the token span of the system prompt as the half-open interval $[s_b, e_b)$, where s_b is the index of the start token and e_b is the index immediately following the end token. The length of the system prompt for that sequence is $\ell_{sys,b} = e_b - s_b$.

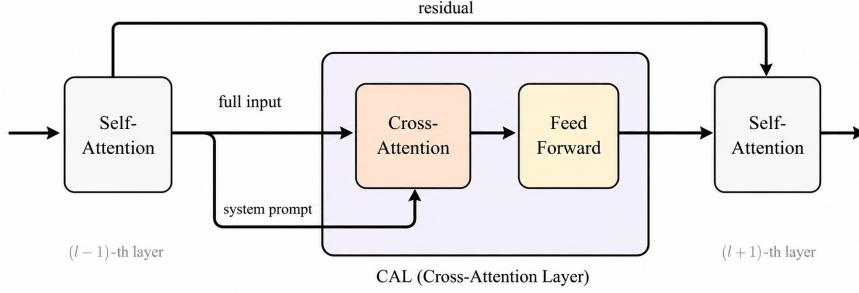


Figure 1: **The CALYREX Architecture.** A CAL block performs cross-attention between the system prompt and the full input. The result is then fed to a feedforward network before the next layer. The CAL block is inserted between normal self-attention blocks and residues can bypass the CAL block.

To structurally enforce system-prompt adherence, we introduce the Cross-Attention Layer (CAL) block. Inserted immediately after a standard self-attention layer, a CAL block consists of two sequential residual sublayers: a causal cross-attention sublayer and a SwiGLU MLP.

Causal Cross-Attention. Let $\mathbf{X} \in \mathbb{R}^{B \times T \times d}$ be the residual stream entering the CAL block. Unlike standard cross-attention which queries an external encoder, CALYREX derives its keys and values exclusively from the system-prompt span of its own normalized residual stream. Consider a single sequence with bounds $[s, e)$ and length $\ell_{sys} = e - s$. The queries are projected from the full sequence, while keys and values are restricted to the system-prompt span:

$$\mathbf{Q} = \bar{\mathbf{X}}\mathbf{W}_Q, \quad \mathbf{K} = \bar{\mathbf{X}}_{[s:e]}\mathbf{W}_K, \quad \mathbf{V} = \bar{\mathbf{X}}_{[s:e]}\mathbf{W}_V$$

where $\bar{\mathbf{X}} = \text{RMSNorm}(\mathbf{X})$, and $\mathbf{W}_Q, \mathbf{W}_K, \mathbf{W}_V \in \mathbb{R}^{d \times d}$ are learned projection matrices.

To preserve the autoregressive property of the decoder, we apply a causal mask to the cross-attention. Let s and $e = s + \ell_{sys}$ denote the absolute start and end positions of the system prompt in the sequence. Queries \mathbf{Q} are projected from all T tokens and indexed by their absolute sequence position $i \in [0, T)$. Keys and values \mathbf{K}, \mathbf{V} are projected only from the ℓ_{sys} system-prompt tokens and stored in a compact buffer indexed by slot $j \in [0, \ell_{sys})$, where slot j corresponds to absolute position $s + j$. The causal rule—a query may only attend to a key that does not come after it—then reads $s + j \leq i$, or equivalently:

$$M_{i,j} = \begin{cases} 0 & \text{if } j \leq i - s \\ -\infty & \text{otherwise} \end{cases}$$

This single formula produces three natural zones. For tokens before the system prompt ($i < s$): $i - s < 0$, so no slot satisfies $j \leq i - s$ —these tokens attend to nothing, consistent with the design assumption that the system prompt always precedes user content. For tokens within the system prompt ($s \leq i < e$): $j \leq i - s < \ell_{sys}$, so each token can only attend to earlier system-prompt tokens—standard causal order within the span. For tokens after the system prompt ($i \geq e$): $i - s \geq \ell_{sys}$, so all $j < \ell_{sys}$ are permitted—the mask is fully open and every user-context or generated token sees the entire system prompt. The residual stream is then updated as:

$$\mathbf{X}' = \mathbf{X} + \text{Attention}(\mathbf{Q}, \mathbf{K}, \mathbf{V}, \mathbf{M})\mathbf{W}_O$$

where $\mathbf{W}_O \in \mathbb{R}^{d \times d}$ is the learned output projection.

Batched Processing and Generation. For heterogeneous batches where samples have system prompts of different lengths, keys and values are zero-padded to the batch’s maximum span length ℓ_{max} , with per-sample masks enforcing both the causal rule ($j \leq i - s_b$ for sample b) and a padding mask that marks slots beyond each sample’s true ℓ_{sys} as $-\infty$.

Feed Forward. To refine the cross-attention output, \mathbf{X}' is passed through a secondary normalization and a standard SwiGLU feed-forward network, followed by a down-projection $\mathbf{W}_D \in \mathbb{R}^{4d \times d}$:

$$\mathbf{X}'' = \mathbf{X}' + \text{SwiGLU}(\text{RMSNorm}(\mathbf{X}'))\mathbf{W}_D$$

Computational and System Efficiency. By architecturally decoupling the system prompt from the user context, CALYREX introduces distinct computational advantages. During inference, the cross-attention Key-Value cache is derived exclusively from the fixed system prompt span, maintaining a strict $O(1)$ memory footprint relative to generation length that accelerates Time-To-First-Token and reduces VRAM pressure.

During training, macroscopic CAL placement allows PyTorch to prune the frozen backbone from the backward graph entirely, reducing backward FLOPs from LoRA’s $\approx 4(N_{base} + N_{train})S$ to $\approx 2N_{train}S$ without activation recomputation (formal analysis in Appendix A.6).

Training To efficiently learn weights for the new injected CAL block, the base model \mathcal{M} is strictly frozen, and gradients are applied exclusively to the CAL adapters (θ_{CAL}). To guarantee that injecting these blocks inflicts no “representation shock” on the backbone, the output projections of both CAL sublayers are strictly zero-initialized prior to training: $\mathbf{W}_O \leftarrow \mathbf{0}$ and $\mathbf{W}_D \leftarrow \mathbf{0}$. Consequently, at initialization step $t = 0$, the block acts as a perfect identity mapping ($\mathbf{X}'' = \mathbf{X}$), making the initial loss mathematically identical to the base model’s loss. This structural pass-through ensures that zero-shot capabilities (e.g., mathematical reasoning, factual recall) are perfectly protected from catastrophic forgetting. The model is trained on a diverse 50,000-sample SFT corpus consisting of general tasks. Extended dataset details are provided in Appendix A.5.

4 Ablation Study: Placement Strategy on 1.5B Backbone

The primary objective of this section is to *locate* the optimal CAL placement on a 1.5B backbone. Specifically, we test the performance of inserting CAL blocks at various network depths, seeking the configuration that best enforces rules. We utilize the 28-layer Qwen2.5-1.5B-Instruct [Qwen Team, 2025] as our frozen backbone to enable rapid architectural ablation.

4.1 Experiment Setup

Control Baselines. To rigorously isolate CALYREX’s structural benefits from both the narrow-corpus fine-tuning penalty and the mere addition of parameters, we evaluate against two baselines. Both are matched to the tunable parameter count of 5 CAL blocks (equivalent to LATE8TH configuration) and trained on the same dataset (the LoRA rank derivation for this parameter match is detailed in Appendix A.4):

- **LoRA Baseline:** A standard full-network LoRA. This baseline reveals how much of the score difference is due to dataset bias and narrow-corpus fine-tuning penalties.
- **ParallelMLP Baseline:** Zero-initialized MLP networks [He et al., 2022] injected parallel to the final eighth of self-attention blocks (matching LATE8TH configuration) and trained on a frozen backbone. This baseline reveals how much of the score difference results from the location of the adapter and frozen backbone rather than the cross-attention architecture.

Configurations. To understand which placement of CAL blocks is most effective, we trained eight CAL placement configurations across the 28-layer backbone. The full list of configurations is detailed in Appendix A.1.

4.2 Empirical Results and Structural Trade-offs

Preservation of General Reasoning. To evaluate foundational semantic preservation, we measure complex mathematical reasoning via GSM8K [Cobbe et al., 2021] and factual recall via MMLU [Hendrycks et al., 2021]. Standard parameter-efficient tuning on narrow instruction distributions naturally induces catastrophic forgetting. This narrow-corpus fine-tuning penalty is evident in the LoRA baseline. Conversely, the frozen-backbone techniques structurally protect these capabilities. Both the ParallelMLP baseline and CALYREX essentially recover full base-model performance.

1.5B CALYREX Configuration Benchmark Results

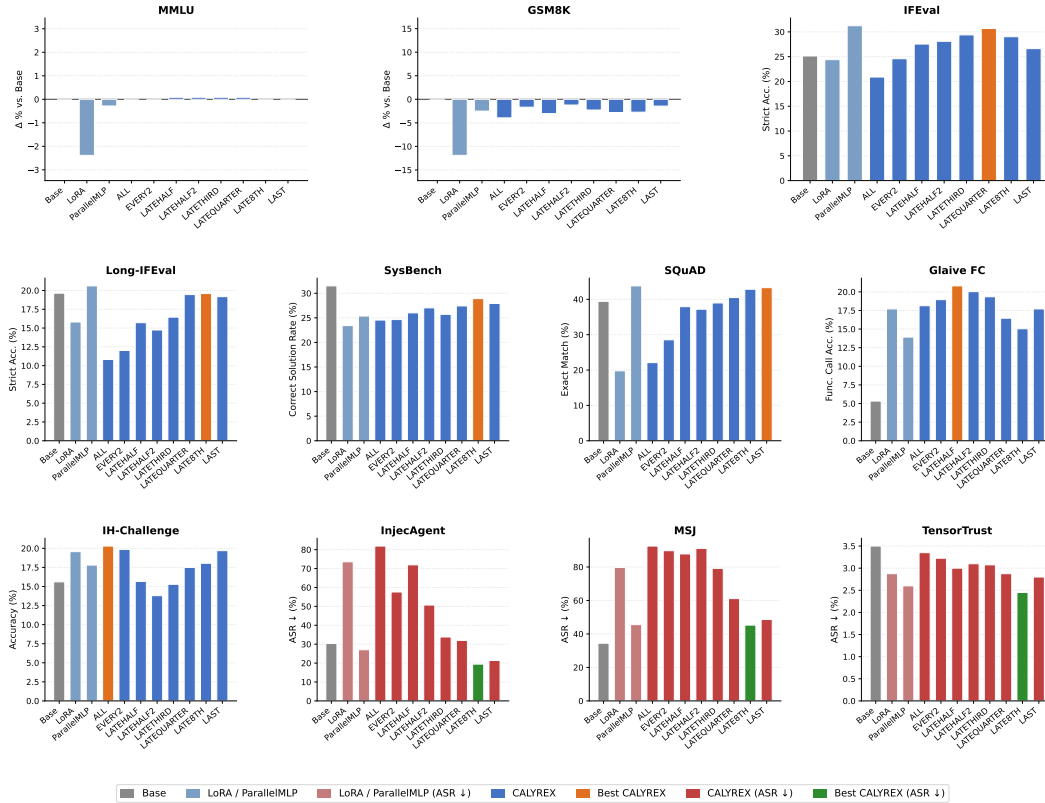


Figure 2: Empirical benchmark results across CAL placement configurations on the Qwen2.5-1.5B-Instruct backbone. Top Left (MMLU & GSM8K): Plotted as relative deviation ($\Delta\%$) from the base model to highlight capability preservation. Other panels: Absolute scores, with blue graphs as task accuracy (higher is better) and red graphs as attack success rates (ASR; lower is better). Exact data is in B.3.

MMLU effectively suffers 0 degradation because the test sets lack a system prompt, causing the CAL blocks to be bypassed entirely.

Strict Instruction and Formatting Adherence. We evaluate verifiable rule-following using **IFEval** [Zhou et al., 2023] for strict formatting constraints, and **Long-IFEval**, which assesses instruction adherence under extended context by injecting long text into standard IFEval prompts. We also measure multi-turn system-prompt adherence via **SysBench** [Qin et al., 2024], strict information extraction via **SQuAD** [Rajpurkar et al., 2018], and JSON structuring via **Glaive FC** [Glaive AI, 2023].

Late-stage and sparse placements consistently outperform early or dense interventions: final-layer cross-attention anchors formatting rules without disrupting early semantic extraction. Distributing adapters across the final fraction (**LATE8TH**) outperforms a single bottleneck (**LAST**). IFEval peaks slightly earlier (**LATEQUARTER**), while Long-IFEval favors **LATE8TH**'s broader distribution at extended context. However, Glaive FC peaks at **LATEHALF** and degrades for late-stage configurations, indicating complex syntax generation requires deeper semantic integration than a final-stage guardrail.

The LoRA baseline confirms a dataset-induced formatting penalty; CALYREX recovers base performance on most tasks. The ParallelMLP baseline performs comparably on basic formatting benchmarks (IFEval, Long-IFEval, SQuAD). However, on tasks requiring persistent contextual awareness—specifically SysBench (multi-turn adherence) and Glaive FC (structured output generation)—CALYREX outperforms ParallelMLP, indicating that querying the isolated system-prompt

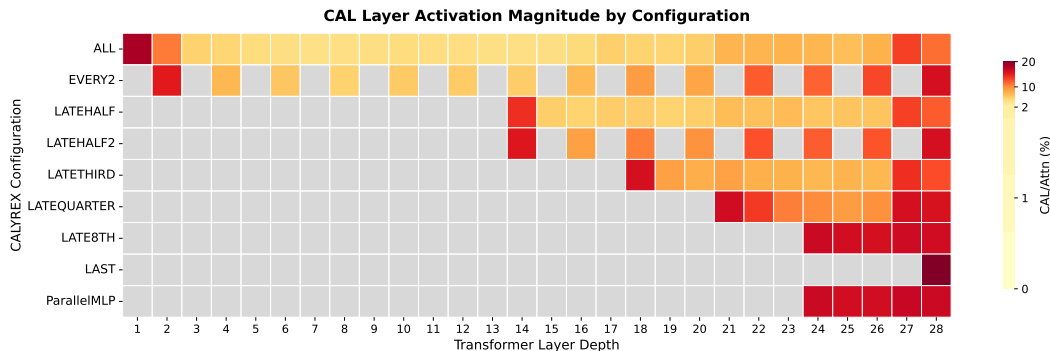


Figure 3: Mechanistic activation magnitude heatmap. Each cell represents the CAL/Attn ℓ_2 norm ratio (%) for a specific configuration (row) at a specific transformer depth (column). Gray cells indicate the absence of a CAL block. All configurations exhibit a U-shaped pattern where early and late layers display higher activation magnitudes than the middle layers, with steep decrease at the start and smooth increase at the end. ParallelMLP shows a late-stage magnitude profile nearly identical to LATE8TH. Exact data is in B.4.

K/V actively prevents semantic override in ways that parallel MLP injection cannot replicate. Although the difference at 1.5B is not significant, this gap widens substantially at 8B, as demonstrated in Section 5.

Prompt Injection and Security. To evaluate structural security, we utilize **IH-Challenge** [Guo et al., 2026] for prioritizing privileged rules over adversarial inputs, **InjecAgent** [Zhan et al., 2024] for indirect prompt injections, **Many-Shot Jailbreaking (MSJ)** [Anil et al., 2024] to test resistance against multi-turn adversarial contents, and **TensorTrust** [Toyer et al., 2024] for interpretable attacks aimed at extracting hidden system instructions.

The security picture mirrors the formatting findings: early-layer cross-attention amplifies attacks (ASR exceeds the LoRA baseline), while late-stage confinement reverses this. IH-Challenge exhibits a U-shaped pattern where both ALL and late-stage placements outperform mid-network configurations, yet late-stage configurations still achieve a comparable score to the ALL configuration.

LoRA fine-tuning on this general-purpose corpus broadly increases ASR, consistent with the known sensitivity of behavioral alignment to training distribution; CALYREX recovers or approaches base-model performance on most attack benchmarks, except on MSJ, where the absence of multi-turn adversarial data depresses all fine-tuned models equally. Critically, at 1.5B, CALYREX LATE8TH beats ParallelMLP across all four security benchmarks—confirming that cross-attention routing, not merely late-stage parameter addition, drives structural prompt-injection resistance.

Based on the benchmark scores, the LATE8TH configuration is the overall best, winning 5 out of 9 benchmarks across all configurations, while keeping tunable parameters low.

4.3 Mechanistic Activation Analysis

To understand the structural causes behind our benchmark results, we probe the internal mechanics of the CAL blocks. We measure the relative activation magnitude by computing the ratio of the ℓ_2 norm of the CAL block’s output delta to the base self-attention output: $\frac{\|\mathbf{X}'' - \mathbf{X}'\|_2}{\|\mathbf{A}_{self}\|_2}$.

Prior work shows that behavioral constraints are predominantly localized in late-stage network depths [Zou et al., 2023, Geva et al., 2022]. Our heatmap (Figure 3) provides empirical validation of this spatial bottleneck and explains performance variance across configurations.

We observe that successful rule-following strongly correlates with sustained activation magnitude in the final layers of the network (Layers 25–28). Successful configurations—EVERY2, LATEHALF2, LATEQUARTER, LATE8TH—all maintain magnitude $> 1\%$ (orange) in late layers (25–28). In the optimal LATE8TH configuration, the activation magnitude remains concentrated in this critical zone,

approaching a healthy 2–4%. This provides the network with sufficient “structural bandwidth” to enforce the system prompt at the exact depth where final behavioral constraints are applied. ParallelMLP’s late-stage magnitude profile is nearly identical to LATE8TH, explaining its competitive performance: spatial locality of rules is a property of the frozen backbone, and any late-stage adapter benefits from this natural enforcement depth.

Dense early-layer placements over-index prematurely, disrupting feature extraction, which leads to a worse score than the LoRA baseline in most benchmarks. In addition, early placements decay in magnitude before reaching the critical late-stage bottleneck, which leads to less influence on rule-following. LAST configuration injects a huge shift across a narrow zone, which degrades the performance. However, LAST still beats early-stage injections for most benchmarks, indicating that a late-stage influence is critical to enhance rule-following.

5 Main Results: 8B Scale Evaluation

The main goal of this section is to study the architectural advantage of CALYREX at scale. However, the difference in score relative to the base model can be attributed to 4 factors: **the training data, the location of the added parameters, the frozen backbone, and the CALYREX architecture.** We utilize the LoRA baseline to isolate dataset bias, and the ParallelMLP baseline to control for parameter location and backbone freezing. Consequently, the explicit architectural contribution is defined by the relative score between CALYREX and ParallelMLP.

Table 1: Benchmark results on 8B models. All values are absolute percentages (%). \uparrow/\downarrow indicates whether higher or lower scores are better. **Bold** figure denotes the better score between ParallelMLP and CALYREX; ** ($p < 0.01$) and * ($p < 0.05$) denote statistical significance (two-sided z -test).

Model	General		Instruction-Following					Security			
	MMLU \uparrow	GSM8K \uparrow	IFEval \uparrow	L-IFEval \uparrow	SysBench \uparrow	SQuAD \uparrow	Glaive \uparrow	IH-Chal. \uparrow	InjecAgent \downarrow	MSJ \downarrow	TensorTrust \downarrow
Base	68.25	85.37	71.16	41.40	60.76	47.50	14.78	11.13	82.00	10.00	7.83
LoRA	64.88	76.95	57.12	34.66	45.82	64.55	21.87	20.79	84.75	73.61	5.05
ParallelMLP	68.01	83.02	61.74	31.84	42.32	59.33	1.89	12.01	71.55**	38.05	7.22
CALYREX (LATE8TH)	68.25	83.02	69.13*	33.92	58.60**	58.75	6.66**	14.14**	81.90	25.00**	6.80

Section 4 identified the LATE8TH configuration as the optimal CAL placement on a 1.5B backbone. We now demonstrate its architectural advantages at scale by evaluating on the Llama-3.1-8B-Instruct [Meta, 2024] backbone using the identical training corpus, comparing against parameter-matched full-network LoRA and late-stage ParallelMLP baselines.

We observe that the performance shifts of both CALYREX and LoRA correlate, confirming that the dataset is the primary driver of score changes relative to the base model. For example, the widespread degradation in the LoRA baseline on general reasoning indicates a dataset-induced behavioral tax. Because CALYREX operates on a frozen backbone, it resists this semantic degradation, explaining its higher scores relative to LoRA. Conversely, this frozen architecture limits behavioral adaptation; on tasks where the SFT dataset actively improves performance (such as the IH-Challenge), CALYREX yields smaller gains than full-network fine-tuning. In both cases, by comparing CALYREX against the ParallelMLP control, we cleanly factor out both dataset bias and frozen-backbone effects, directly isolating the structural advantages of the cross-attention architecture.

Scale-Dependent Widening of the Architectural Gap. The 1.5B results of Section 4 showed that CALYREX and ParallelMLP perform comparably on most instruction-following benchmarks. At 8B, this gap widens substantially. On IFEval, CALYREX trails ParallelMLP by 2.2% at 1.5B but leads by +7.4% at 8B. On SysBench, the CALYREX advantage over ParallelMLP grows from +3.5% to +16.3%. On Many-Shot Jailbreaking, CALYREX reduces the attack success rate by 13.1% below ParallelMLP at 8B, compared to a slight advantage at 1.5B. While based on only two scales, this widening is consistent with larger backbones more effectively utilizing the dedicated system-prompt K/V pathway.

Architectural Advantages and Limitations. At the 8B scale, CALYREX exhibits a distinct architectural advantage over ParallelMLP across instruction-following benchmarks, significantly outperforming it on IFEval, SysBench, and Glaive FC, with SQuAD as the sole exception. On Long-IFEval, CALYREX shows a modest advantage over ParallelMLP at mid-range context lengths,

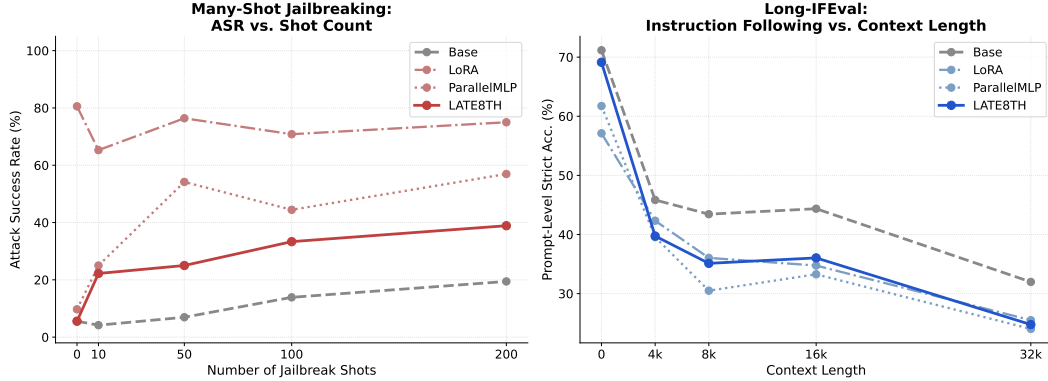


Figure 4: Structural resistance to adversarial and contextual degradation at 8B scale. **Left:** Attack Success Rate (ASR) as a function of in-context Many-Shot Jailbreak demonstrations (lower is better). **Right:** Long-IFEval strict accuracy over extended context windows (4k to 32k tokens). Detailed data in Table 5 and Table 6.

though all fine-tuned models converge at extreme lengths (Figure 4). Neither frozen-backbone method matches LoRA on complex JSON generation, confirming that mastering unfamiliar structural syntax requires full-network semantic modification. The architectural benefit also extends to direct adversarial vectors: CALYREX maintains robustness over ParallelMLP on Many-Shot Jailbreaking and IH-Challenge.

Contextual Degradation Analysis. Figure 4 shows structural resistance to increasing in-context pressure at 8B scale on MSJ and Long-IFEval. LoRA collapses to high ASR even at 0-shot due to the dataset-induced alignment penalty. CALYREX tracks the base model at low shot counts and maintains a substantially lower ASR than ParallelMLP across the full shot range, with the gap most pronounced at 50-shot where adversarial demonstrations begin to accumulate. On Long-IFEval, all fine-tuned models converge at 32K; CALYREX shows a modest advantage over ParallelMLP at 8K and 16K, but no clear separation holds at extreme lengths.

Injec Agent Analysis The InjecAgent reversal at 8B (81.90% vs. 71.55% ASR) is a capability artifact rather than a security gap (Appendix B.2). InjecAgent measures whether a model executes maliciously injected tool calls; consequently, an inability to properly format or trigger tools artificially lowers the ASR. The 8B backbone is highly capable (Valid Rate > 42%) and overwhelmingly compliant (native ASR 82.00%). Because the benchmark uses standard operational system prompts that lack explicit defensive rules against untrusted data, CALYREX structurally anchors the “helpful agent” persona. Without a counter-rule to enforce, it faithfully preserves the backbone’s innate vulnerability (81.90%). This symmetrically explains the low ASR in all 1.5B models, where a low Valid Rate ($\approx 19\%$) indicates general tool-execution failure rather than true security. Critically, ParallelMLP’s lower ASR at 8B does not reflect active defense; it stems from a generalized degradation in tool execution fidelity (e.g., -15.2% on Base Direct Harm relative to CALYREX), meaning it simply fails to execute the complex malicious calls. This reveals a strict boundary condition for structural routing: isolating the system prompt only mitigates prompt injections if the prompt itself explicitly defines defensive boundaries.

Across the two tested scales, CALYREX’s definitive advantages over ParallelMLP are on SysBench, IFEval, and Long-IFEval for instruction adherence and on Many-Shot Jailbreaking for adversarial resistance, with the margins on these benchmarks widening substantially at 8B scale.

6 Discussion and Limitations

CALYREX’s architectural advantages are not perfectly uniform; we observed the following limitations:

- **Task-Specific Gaps:** CALYREX shows no consistent advantage on strict information extraction (SQuAD), where ParallelMLP performs comparably or better at both scales. On GlaiVe FC, both frozen-backbone methods fail to achieve meaningful performance relative to full-network LoRA or even the untuned base, indicating that complex JSON synthesis requires primary semantic pathway modification that isolated late-stage routing cannot provide. On direct adversarial benchmarks, IH-Challenge and TensorTrust show no significant or consistent improvement over ParallelMLP across scales, suggesting that structural cross-attention anchoring does not reliably generalize to all prompt-injection threat surfaces without explicit defensive system prompts.
- **Inconsistent Configuration Dominance:** CALYREX’s best configuration is not uniform. At 1.5B, ALL outperforms LATE8TH on IH-Challenge, LATEHALF wins LATE8TH on GlaiVe function calling.
- **Scaling Verification:** Whether the final-eighth spatial locality of rule-following constraints remains optimal at frontier scales (70B+) requires further verification.
- **Corpus Confound:** All comparisons are conditional on the 50K-sample corpus. A richer or adversarially diverse training set may narrow or widen the gap; results do not generalize to production-scale training. The absence of long-context and multi-turn adversarial data depressed absolute Long-IFEval, SysBench and MSJ scores for all fine-tuned models.

Future Directions. Currently, CALYREX relies on standard Supervised Fine-Tuning (SFT) over a general corpus; at 8B scale, this approach rarely beats the extensively trained base model. Since the 50k-sample corpus already beats the 1.5B base model on most tasks, we hypothesize that, on 8B or larger models, advanced alignment techniques—such as Reinforcement Learning from Human Feedback (RLHF) [Ouyang et al., 2022] or Direct Preference Optimization (DPO) [Rafailov et al., 2023]—explicitly targeted at the CAL blocks would yield substantially stronger results. Moving beyond brute-force SFT could significantly enhance the adapter’s ability to enforce rigid formatting, handle multi-turn adherence, and execute complex safety guardrails.

Additionally, CALYREX introduces a generalized methodology for structurally separating hierarchical context. Rather than flattening heterogeneous inputs into a single dilutable stream, future architectures could extend this late-stage, zero-initialized cross-attention approach to dynamically route and merge other distinct data tiers—such as massive external knowledge bases or retrieved documents—preventing the vulnerabilities inherent to uniform attention.

Broader Impacts. CALYREX reduces prompt injection vulnerability in safety-critical AI deployments, supporting responsible use in multi-turn and agentic applications. Publishing attack-success-rate analyses may inform adversaries; however, all benchmarks used are existing public resources and this paper introduces no new attack methods. Enhanced instruction-following could also be exploited if a system prompt itself contains harmful directives—a risk shared by all behavioral alignment approaches.

7 Conclusion

We introduce **CALYREX**, an architecture that uses cross-attention to structurally isolate the system prompt, addressing the Instruction Hierarchy problem. A placement ablation on a 1.5B backbone identifies the final eighth of layers as optimal, where behavioral constraints are naturally concentrated.

Within the frozen-backbone fine-tuning regime, CALYREX outperforms parameter-matched structural baselines on instruction-following (IFEval, Long-IFEval, SysBench) and many-shot jailbreak resistance (MSJ), while showing no consistent advantage on strict extraction (SQuAD) or direct-attack security benchmarks (IH-Challenge, TensorTrust). The limited corpus coverage remains the binding constraint preventing it from matching the untuned base model. The structural gap over ParallelMLP appears to widen with model scale at the two tested parameter counts, consistent with larger backbones more effectively leveraging a dedicated system-prompt routing pathway.

Acknowledgments and Disclosure of Funding

[Omitted in anonymized submission.]

References

- Sahar Abdelnabi, Kai Greshake, Shailesh Mishra, Christoph Endres, Thorsten Holz, and Mario Fritz. Not what you’ve signed up for: Compromising real-world llm-integrated applications with indirect prompt injection. In Maura Pintor, Xinyun Chen, and Florian Tramèr, editors, *Proceedings of the 16th ACM Workshop on Artificial Intelligence and Security, AISec 2023, Copenhagen, Denmark, 30 November 2023*, pages 79–90. ACM, 2023. doi: 10.1145/3605764.3623985. URL <https://doi.org/10.1145/3605764.3623985>.
- Jean-Baptiste Alayrac, Jeff Donahue, Pauline Luc, Antoine Miech, Iain Barr, Yana Hasson, Karel Lenc, Arthur Mensch, Katherine Millican, Malcolm Reynolds, Roman Ring, Eliza Rutherford, Serkan Cabi, Tengda Han, Zhitao Gong, Sina Samangooei, Marianne Monteiro, Jacob L. Menick, Sebastian Borgeaud, Andy Brock, Aida Nematzadeh, Sahand Sharifzadeh, Mikolaj Binkowski, Ricardo Barreira, Oriol Vinyals, Andrew Zisserman, and Karén Simonyan. Flamingo: a visual language model for few-shot learning. In Sanmi Koyejo, S. Mohamed, A. Agarwal, Danielle Belgrave, K. Cho, and A. Oh, editors, *Advances in Neural Information Processing Systems 35: Annual Conference on Neural Information Processing Systems 2022, NeurIPS 2022, New Orleans, LA, USA, November 28 - December 9, 2022*, 2022. URL http://papers.nips.cc/paper_files/paper/2022/hash/960a172bc7fbf0177cccb411a7d800-Abstract-Conference.html.
- Cem Anil, Esin Durmus, Nina Panickssery, Mrinank Sharma, Joe Benton, Sandipan Kundu, Joshua Batson, Meg Tong, Jesse Mu, Daniel Ford, Francesco Mosconi, Rajashree Agrawal, Rylan Schaeffer, Naomi Bashkansky, Samuel Svenningsen, Mike Lambert, Ansh Radhakrishnan, Carson Denison, Evan Hubinger, Yuntao Bai, Trenton Bricken, Timothy Maxwell, Nicholas Schiefer, James Sully, Alex Tamkin, Tamera Lanham, Karina Nguyen, Tomek Korbak, Jared Kaplan, Deep Ganguli, Samuel R. Bowman, Ethan Perez, Roger B. Grosse, and David Kristjanson Duvenaud. Many-shot jailbreaking. In Amir Globersons, Lester Mackey, Danielle Belgrave, Angela Fan, Ulrich Paquet, Jakub M. Tomczak, and Cheng Zhang, editors, *Advances in Neural Information Processing Systems 38: Annual Conference on Neural Information Processing Systems 2024, NeurIPS 2024, Vancouver, BC, Canada, December 10 - 15, 2024*, 2024. URL http://papers.nips.cc/paper_files/paper/2024/hash/ea456e232efb72d261715e33ce25f208-Abstract-Conference.html.
- Sizhe Chen, Julien Piet, Chawin Sitawarin, and David A. Wagner. Struq: Defending against prompt injection with structured queries. In Lujo Bauer and Giancarlo Pellegrino, editors, *34th USENIX Security Symposium, USENIX Security 2025, Seattle, WA, USA, August 13-15, 2025*, pages 2383–2400. USENIX Association, 2025a. URL <https://www.usenix.org/conference/usenixsecurity25/presentation/chen-sizhe>.
- Sizhe Chen, Arman Zharmagambetov, Saeed Mahloujifar, Kamalika Chaudhuri, David A. Wagner, and Chuan Guo. Secalign: Defending against prompt injection with preference optimization. In Chun-Ying Huang, Jyh-Cheng Chen, Shih-Pyng Shieh, David Lie, and Véronique Cortier, editors, *Proceedings of the 2025 ACM SIGSAC Conference on Computer and Communications Security, CCS 2025, Taipei, Taiwan, October 13-17, 2025*, pages 2833–2847. ACM, 2025b. doi: 10.1145/3719027.3744836. URL <https://doi.org/10.1145/3719027.3744836>.
- Karl Cobbe, Vineet Kosaraju, Mohammad Bavarian, Mark Chen, Heewoo Jun, Lukasz Kaiser, Matthias Plappert, Jerry Tworek, Jacob Hilton, Reiichiro Nakano, Christopher Hesse, and John Schulman. Training verifiers to solve math word problems. *CoRR*, abs/2110.14168, 2021. URL <https://arxiv.org/abs/2110.14168>.
- Jon Durbin. Airoboros: A diverse, synthetically generated dataset for instruction tuning, 2023. URL <https://huggingface.co/datasets/jondurbin/airoboros-3.2>.
- Mor Geva, Avi Caciularu, Kevin Ro Wang, and Yoav Goldberg. Transformer feed-forward layers build predictions by promoting concepts in the vocabulary space. In Yoav Goldberg, Zornitsa Kozareva, and Yue Zhang, editors, *Proceedings of the 2022 Conference on Empirical Methods in Natural Language Processing, EMNLP 2022, Abu Dhabi, United Arab Emirates, December 7-11, 2022*, pages 30–45. Association for Computational Linguistics, 2022. doi: 10.18653/V1/2022.EMNLP-MAIN.3. URL <https://doi.org/10.18653/v1/2022.emnlp-main.3>.
- Glaive AI. Glaive function calling v2. <https://huggingface.co/datasets/glaiveai/glaive-function-calling-v2>, 2023. HuggingFace dataset.

- Chuan Guo, Juan Felipe Ceron Uribe, Sicheng Zhu, Christopher A. Choquette-Choo, Stephanie Lin, Nikhil Kandpal, Milad Nasr, Rai, Sam Toyer, Miles Wang, Yaodong Yu, Alex Beutel, and Kai Xiao. Ih-challenge: A training dataset to improve instruction hierarchy on frontier llms. *CoRR*, abs/2603.10521, 2026. doi: 10.48550/ARXIV.2603.10521. URL <https://doi.org/10.48550/arXiv.2603.10521>.
- Junxian He, Chunting Zhou, Xuezhe Ma, Taylor Berg-Kirkpatrick, and Graham Neubig. Towards a unified view of parameter-efficient transfer learning. In *The Tenth International Conference on Learning Representations, ICLR 2022, Virtual Event, April 25-29, 2022*. OpenReview.net, 2022. URL <https://openreview.net/forum?id=ORDcd5Axok>.
- Dan Hendrycks, Collin Burns, Steven Basart, Andy Zou, Mantas Mazeika, Dawn Song, and Jacob Steinhardt. Measuring massive multitask language understanding. In *9th International Conference on Learning Representations, ICLR 2021, Virtual Event, Austria, May 3-7, 2021*. OpenReview.net, 2021. URL <https://openreview.net/forum?id=d7KBjmI3GmQ>.
- Edward J. Hu, Yelong Shen, Phillip Wallis, Zeyuan Allen-Zhu, Yuanzhi Li, Shean Wang, Lu Wang, and Weizhu Chen. Lora: Low-rank adaptation of large language models. In *The Tenth International Conference on Learning Representations, ICLR 2022, Virtual Event, April 25-29, 2022*. OpenReview.net, 2022. URL <https://openreview.net/forum?id=nZeVKeeFYf9>.
- Jiaming Ji, Mickel Liu, Josef Dai, Xuehai Pan, Chi Zhang, Ce Bian, Boyuan Chen, Ruiyang Sun, Yizhou Wang, and Yaodong Yang. Beavertails: Towards improved safety alignment of llm via a human-preference dataset. *Advances in Neural Information Processing Systems*, 36, 2024.
- Junnan Li, Dongxu Li, Silvio Savarese, and Steven C. H. Hoi. BLIP-2: bootstrapping language-image pre-training with frozen image encoders and large language models. In Andreas Krause, Emma Brunskill, Kyunghyun Cho, Barbara Engelhardt, Sivan Sabato, and Jonathan Scarlett, editors, *International Conference on Machine Learning, ICML 2023, 23-29 July 2023, Honolulu, Hawaii, USA*, Proceedings of Machine Learning Research, pages 19730–19742. PMLR, 2023. URL <https://proceedings.mlr.press/v202/li23q.html>.
- Ilya Loshchilov and Frank Hutter. Decoupled weight decay regularization. In *7th International Conference on Learning Representations, ICLR 2019, New Orleans, LA, USA, May 6-9, 2019*. OpenReview.net, 2019. URL <https://openreview.net/forum?id=Bkg6RiCqY7>.
- Meta. The llama 3 herd of models, 2024. URL <https://arxiv.org/abs/2407.21783>.
- Long Ouyang, Jeffrey Wu, Xu Jiang, Diogo Almeida, Carroll L. Wainwright, Pamela Mishkin, Chong Zhang, Sandhini Agarwal, Katarina Slama, Alex Ray, John Schulman, Jacob Hilton, Fraser Kelton, Luke Miller, Maddie Simens, Amanda Askell, Peter Welinder, Paul F. Christiano, Jan Leike, and Ryan Lowe. Training language models to follow instructions with human feedback. In Sanmi Koyejo, S. Mohamed, A. Agarwal, Danielle Belgrave, K. Cho, and A. Oh, editors, *Advances in Neural Information Processing Systems 35: Annual Conference on Neural Information Processing Systems 2022, NeurIPS 2022, New Orleans, LA, USA, November 28 - December 9, 2022*, 2022. URL http://papers.nips.cc/paper_files/paper/2022/hash/b1efde53be364a73914f58805a001731-Abstract-Conference.html.
- Fábio Perez and Ian Ribeiro. Ignore previous prompt: Attack techniques for language models. *CoRR*, abs/2211.09527, 2022. doi: 10.48550/ARXIV.2211.09527. URL <https://doi.org/10.48550/arXiv.2211.09527>.
- Yanzhao Qin, Tao Zhang, Yanjun Shen, Wenjing Luo, Haoze Sun, Yan Zhang, Yujing Qiao, Weipeng Chen, Zenan Zhou, Wentao Zhang, and Bin Cui. Sysbench: Can large language models follow system messages? *CoRR*, abs/2408.10943, 2024. doi: 10.48550/ARXIV.2408.10943. URL <https://doi.org/10.48550/arXiv.2408.10943>.
- Qwen Team. Qwen2.5 technical report. *arXiv preprint arXiv:2412.15115*, 2025.
- Rafael Rafailov, Archit Sharma, Eric Mitchell, Christopher D. Manning, Stefano Ermon, and Chelsea Finn. Direct preference optimization: Your language model is secretly a reward model. In Alice Oh, Tristan Naumann, Amir Globerson, Kate Saenko, Moritz Hardt, and Sergey Levine,

- editors, *Advances in Neural Information Processing Systems 36: Annual Conference on Neural Information Processing Systems 2023, NeurIPS 2023, New Orleans, LA, USA, December 10 - 16, 2023*, 2023. URL http://papers.nips.cc/paper_files/paper/2023/hash/a85b405ed65c6477a4fe8302b5e06ce7-Abstract-Conference.html.
- Samyam Rajbhandari, Jeff Rasley, Olatunji Ruwase, and Yuxiong He. Zero: memory optimizations toward training trillion parameter models. In Christine Cuicchi, Irene Qualters, and William T. Kramer, editors, *Proceedings of the International Conference for High Performance Computing, Networking, Storage and Analysis, SC 2020, Virtual Event / Atlanta, Georgia, USA, November 9-19, 2020*, page 20. IEEE/ACM, 2020. doi: 10.1109/SC41405.2020.00024. URL <https://doi.org/10.1109/SC41405.2020.00024>.
- Pranav Rajpurkar, Robin Jia, and Percy Liang. Know what you don't know: Unanswerable questions for squad. In Iryna Gurevych and Yusuke Miyao, editors, *Proceedings of the 56th Annual Meeting of the Association for Computational Linguistics, ACL 2018, Melbourne, Australia, July 15-20, 2018, Volume 2: Short Papers*, pages 784–789. Association for Computational Linguistics, 2018. doi: 10.18653/V1/P18-2124. URL <https://aclanthology.org/P18-2124/>.
- Teknium. Openhermes 2.5: An open dataset of synthetic data for generalist llm assistants, 2023. URL <https://huggingface.co/datasets/teknium/OpenHermes-2.5>.
- Sam Toyer, Olivia Watkins, Ethan Adrian Mendes, Justin Svegliato, Luke Bailey, Tiffany Wang, Isaac Ong, Karim Elmaaroufi, Pieter Abbeel, Trevor Darrell, Alan Ritter, and Stuart Russell. Tensor trust: Interpretable prompt injection attacks from an online game. In *The Twelfth International Conference on Learning Representations, ICLR 2024, Vienna, Austria, May 7-11, 2024*. OpenReview.net, 2024. URL <https://openreview.net/forum?id=fsW7wJGLBd>.
- Ashish Vaswani, Noam Shazeer, Niki Parmar, Jakob Uszkoreit, Llion Jones, Aidan N. Gomez, Lukasz Kaiser, and Illia Polosukhin. Attention is all you need. In Isabelle Guyon, Ulrike von Luxburg, Samy Bengio, Hanna M. Wallach, Rob Fergus, S. V. N. Vishwanathan, and Roman Garnett, editors, *Advances in Neural Information Processing Systems 30: Annual Conference on Neural Information Processing Systems 2017, December 4-9, 2017, Long Beach, CA, USA*, pages 5998–6008, 2017. URL <https://proceedings.neurips.cc/paper/2017/hash/3f5ee243547dee91fbd053c1c4a845aa-Abstract.html>.
- Eric Wallace, Kai Xiao, Reimar Leike, Lilian Weng, Johannes Heidecke, and Alex Beutel. The instruction hierarchy: Training llms to prioritize privileged instructions. *CoRR*, abs/2404.13208, 2024. doi: 10.48550/ARXIV.2404.13208. URL <https://doi.org/10.48550/arXiv.2404.13208>.
- Qiusi Zhan, Zhixiang Liang, Zifan Ying, and Daniel Kang. Injecagent: Benchmarking indirect prompt injections in tool-integrated large language model agents. In Lun-Wei Ku, Andre Martins, and Vivek Srikumar, editors, *Findings of the Association for Computational Linguistics, ACL 2024, Bangkok, Thailand and virtual meeting, August 11-16, 2024*, Findings of ACL, pages 10471–10506. Association for Computational Linguistics, 2024. doi: 10.18653/V1/2024.FINDINGS-ACL.624. URL <https://doi.org/10.18653/v1/2024.findings-acl.624>.
- Lvmin Zhang, Anyi Rao, and Maneesh Agrawala. Adding conditional control to text-to-image diffusion models. In *IEEE/CVF International Conference on Computer Vision, ICCV 2023, Paris, France, October 1-6, 2023*, pages 3813–3824. IEEE, 2023. doi: 10.1109/ICCV51070.2023.00355. URL <https://doi.org/10.1109/ICCV51070.2023.00355>.
- Jeffrey Zhou, Tianjian Lu, Swaroop Mishra, Siddhartha Brahma, Sujoy Basu, Yi Luan, Denny Zhou, and Le Hou. Instruction-following evaluation for large language models. *CoRR*, abs/2311.07911, 2023. doi: 10.48550/ARXIV.2311.07911. URL <https://doi.org/10.48550/arXiv.2311.07911>.
- Andy Zou, Long Phan, Sarah Li Chen, James Campbell, Phillip Guo, Richard Ren, Alexander Pan, Xuwang Yin, Mantas Mazeika, Ann-Kathrin Dombrowski, Shashwat Goel, Nathaniel Li, Michael J. Byun, Zifan Wang, Alex Mallen, Steven Basart, Sanmi Koyejo, Dawn Song, Matt Fredrikson, J. Zico Kolter, and Dan Hendrycks. Representation engineering: A top-down approach to AI transparency. *CoRR*, abs/2310.01405, 2023. doi: 10.48550/ARXIV.2310.01405. URL <https://doi.org/10.48550/arXiv.2310.01405>.

A Implementation Details

The following subsections detail the CAL placement configurations evaluated in Section 4 (§A.1), full training hyperparameters (§A.2), dataset composition (§A.5), system-prompt span detection (§A.3), LoRA parameter matching (§A.4), and training speed analysis (§A.6).

A.1 CALYREX Configurations

Table 2 lists the eight specific CAL placement strategies evaluated across the 28-layer backbone to map the spatial locality of system-prompt constraints.

Configuration	Placement Strategy	Blocks ($ \mathcal{P} $)
ALL	After every layer	28
EVERY2	After every other layer	14
LATEHALF	Distributed across the last $\frac{1}{2}$ of layers, contiguous	15
LATEHALF2	Interleaved throughout the last $\frac{1}{2}$ of layers	8
LATETHIRD	Distributed across the last $\frac{1}{3}$ of layers	11
LATEQUARTER	Distributed across the last $\frac{1}{4}$ of layers	8
LATE8TH	Distributed across the last $\frac{1}{8}$ of layers	5
LAST	A single block after the final layer	1

Table 2: Detailed CAL placement configurations evaluated on the 28-layer Qwen2.5-1.5B-Instruct backbone.

A.2 Training Hyperparameters and Hardware

Table 3 lists the full set of hyperparameters used to train the CAL adapter layers for both experimental phases. All runs use a cosine learning-rate schedule with a linear warmup phase, fused AdamW [Loshchilov and Hutter, 2019], and bfloat16 mixed precision. Training is distributed via DeepSpeed ZeRO Stage 2 [Rajbhandari et al., 2020] with CPU optimizer-state offload, which reduces peak VRAM by approximately 50% compared to a standard data-parallel setup. Gradient checkpointing is deliberately disabled: because CAL adapters sit outside the frozen backbone’s computation graph, intermediate backbone activations can be discarded immediately during the forward pass without affecting gradient flow through the adapters (see Section 3). All model training, ablation runs, and benchmark evaluations were conducted using NVIDIA A100 80GB hardware, requiring approximately 20 total compute days across the project. The backbone models are used under their respective licenses: Qwen2.5-1.5B-Instruct is released under the Apache 2.0 license; Llama-3.1-8B-Instruct is released under the Llama 3.1 Community License.

A.3 System Prompt Span Detection

CAL blocks require the token-level span $[s, e)$ of the system prompt at runtime. The following procedure is applied at every prefill step, supporting the ChatML format used by Qwen [Qwen Team, 2025] and the header format used by Llama 3 [Meta, 2024]. The returned interval is left-closed, right-open (Python-slice convention): `hidden_states[:, s:e, :]` spans from the opening delimiter through the closing delimiter inclusive.

1. Decode each token t_i in the sequence to its string representation.
2. **Start detection:** if "system" appears in the current decoded string *and* the previous token string is `<|im_start|>` (ChatML) or `<|start_header_id|>` (Llama-3 header), record $s = i - 1$ (the inclusive index of the opening delimiter).
3. **End detection:** once inside the system-prompt span, if the current token string contains `<|im_end|>` or `<|eot_id|>`, record $e = i + 1$ (one past the closing delimiter) and return (s, e) .
4. If no system prompt is found, return $(0, 0)$; the CAL cross-attention is a no-op for that sample and its output is zero-masked.

Setting	Qwen2.5-1.5B	Llama-3.1-8B
Learning rate	2×10^{-4}	5×10^{-5}
LR schedule	cosine	cosine
Warmup ratio	0.05	0.10
Weight decay	0.01	0.01
Optimizer	AdamW (fused)	AdamW (fused)
Per-device batch size	4	4
Gradient accumulation steps	32	32
Effective batch size	128	128
Max gradient norm	1.0	0.5
Training epochs	2	2
Max sequence length (tokens)	2,048	2,048
Precision	bfloat16	bfloat16
Gradient checkpointing	disabled	disabled

Table 3: Full training hyperparameter settings for each backbone. The conservative Llama 3.1 settings (lower LR, longer warmup, tighter gradient clipping) mitigate catastrophic forgetting in the larger model.

For batched inference, `get_batch_sys_bounds` applies this procedure to each row and returns a LongTensor of shape $(B, 2)$. Rows with no system prompt receive $[0, 0]$. Span boundaries are cached after the prefill step and reused for all subsequent autoregressive decoding steps without recomputation.

A.4 LoRA Baseline Parameter Matching

The LoRA [Hu et al., 2022] baselines are parameter-matched to the corresponding CALYREX configuration. Given the base model’s hidden dimension H , GQA KV dimension d_{kv} , and feed-forward intermediate size I , the equal-rank solution across all n layers is:

$$r = \left\lfloor \frac{P_{\text{target}}}{n \cdot (2(H + d_{kv}) + 4H + 3(H + I))} \right\rfloor \quad (1)$$

where P_{target} is the trainable parameter budget of the matched CALYREX configuration and $\lfloor \cdot \rfloor$ denotes rounding to the nearest integer. When $r > d_{kv}$ (the GQA KV-projection ceiling), `k_proj` and `v_proj` are capped at rank d_{kv} and the residual budget is redistributed to the remaining modules. All LoRA adapters target the seven linear projections in each transformer block (`q_proj`, `k_proj`, `v_proj`, `o_proj`, `gate_proj`, `up_proj`, `down_proj`), use $\alpha = 2r$, and apply zero dropout.

Equation (1) evaluates to $r = 64$ ($\alpha = 128$) for the Qwen2.5-1.5B micro-analysis (Section 4) and hits the implementation cap of 512 for the Llama-3.1-8B macro-evaluation (Section 5), yielding $r = 512$ ($\alpha = 1024$).

A.5 Dataset Composition

Table 4 lists the exact sample counts per source after filtering. Sequences exceeding the 2,048-token limit are truncated; no padding is applied during tokenization. All sources are shuffled with seed 42 before selection.

A.6 Training Speed Analysis

Section 3 argues that CALYREX’s macroscopic adapter placement enables faster training than LoRA by eliminating the need to backpropagate through the frozen backbone. We provide a formal FLOP analysis here.

Let P_b denote the frozen base model parameter count, P_a the adapter parameter count (equal for CALYREX and LoRA by construction), and S the sequence length. Under the standard approximation that the backward pass requires $2\times$ the FLOPs of the forward pass through the same parameters:

Source	Samples	Filter / selection rule	License
OpenHermes-2.5 [Teknium, 2023]	20,000	Rows grouped by unique system-prompt text; examples drawn by round-robin across groups to maximize system-prompt diversity. Rows lacking a system turn receive the default prompt “ <i>You are a helpful AI assistant.</i> ”	Mixed / unspecified
Airoboros-3.2 [Durbin, 2023]	20,000	Rows must include all three conversation roles (system, human, gpt); qualifying rows are shuffled and the first 20,000 retained.	CC BY 4.0
PKU-SafeRLHF [Ji et al., 2024]	10,000	Only rows where the higher-quality (chosen) response satisfies <code>is_safe=True</code> and <code>severity_level=0</code> (both fields refer to the chosen response) are retained. Per-example system prompt randomly drawn from a pool of 20 distinct safety phrasings to prevent the CAL layer from memorizing a fixed phrasing.	CC BY-NC 4.0
Total	50,000		

Table 4: SFT corpus composition (40% OpenHermes / 40% Airoboros / 20% PKU-SafeRLHF).

CALYREX. The base model is frozen and all adapters sit outside the backbone’s autograd graph. PyTorch prunes frozen nodes from the computation graph entirely when `requires_grad=False` is set on all frozen parameters, which our implementation enforces—the FLOP analysis in Equation (6) predicts a $\sim 3\times$ per-step speedup in the $P_b \gg P_a$ limit. The backward pass flows only through the adapter layers:

$$\mathcal{F}_{\text{CALYREX}}^{\text{back}} = 2 P_a S. \quad (2)$$

LoRA. Even though the base weights are frozen, the chain rule requires propagating the input-activation gradient $\partial\mathcal{L}/\partial\mathbf{x}_i$ through all base layers to reach LoRA adapters inserted at intermediate positions. Because the resulting activation memory exceeds typical VRAM budgets at 8B+ scale,¹ gradient checkpointing is required, adding one full forward-recompute pass:

$$\mathcal{F}_{\text{LoRA}}^{\text{back}} = 4 (P_b + P_a) S. \quad (3)$$

Total per-sample FLOPs (shared forward pass plus respective backward passes):

$$\mathcal{F}_{\text{CALYREX}} = 2(P_b + P_a)S + 2 P_a S, \quad (4)$$

$$\mathcal{F}_{\text{LoRA}} = 2(P_b + P_a)S + 4(P_b + P_a)S = 6(P_b + P_a)S. \quad (5)$$

The theoretical per-step speedup ratio is therefore:

$$\rho = \frac{\mathcal{F}_{\text{LoRA}}}{\mathcal{F}_{\text{CALYREX}}} = \frac{6(P_b + P_a)}{2(P_b + P_a) + 2 P_a}. \quad (6)$$

In the limit $P_b \gg P_a$, $\rho \rightarrow 3$; as $P_a \rightarrow P_b$, $\rho \rightarrow 2$. Both bounds hold regardless of model architecture.

¹Gradient checkpointing may not be required on machines with sufficient VRAM; it is nonetheless standard practice for LoRA training at 8B+ parameter scale and is the assumption used in our evaluation.

B Additional Results

B.1 MSJ and Long-IFEVAL Scores Detail

Table 5: MSJ attack success rate (%) by in-context shot count. Lower is better.

Model	0-shot	10-shot	50-shot	100-shot	200-shot
<i>1.5B models</i>					
Base	2.8	34.7	41.7	55.6	37.5
LoRA	91.7	73.6	77.8	75.0	80.6
ParMLP	13.9	41.7	47.2	65.3	59.7
ALL	91.7	94.4	93.1	91.7	91.7
EVERY2	88.9	90.3	91.7	88.9	88.9
L-HALF	77.8	86.1	90.3	94.4	90.3
L-HALF2	91.7	93.1	91.7	90.3	88.9
L-THIRD	66.7	81.9	83.3	83.3	80.6
L-QUART	34.7	59.7	69.4	76.4	65.3
L-8TH	26.4	44.4	54.2	55.6	45.8
LAST	29.2	44.4	56.9	61.1	51.4
<i>8B models</i>					
Base-8B	5.6	4.2	6.9	13.9	19.4
LoRA-8B	80.6	65.3	76.4	70.8	75.0
ParMLP-8B	9.7	25.0	54.2	44.4	56.9
L-8TH-8B	5.6	22.2	25.0	33.3	38.9

Table 6: IFEval prompt-level strict accuracy (%) by context length. Higher is better.

Model	Std	4K	8K	16K	32K
<i>1.5B models</i>					
Base	25.1	20.0	21.6	22.4	14.6
LoRA	24.4	20.7	19.2	12.8	10.5
ParMLP	31.2	19.6	22.6	23.8	16.5
ALL	20.9	13.9	9.2	12.9	7.2
EVERY2	24.6	16.1	9.4	13.9	8.7
L-HALF	27.5	16.3	18.7	17.6	10.4
L-HALF2	28.1	15.0	17.0	16.8	10.2
L-THIRD	29.4	18.3	18.5	18.9	10.2
L-QUART	30.7	18.7	22.2	23.1	13.9
L-8TH	29.0	18.3	22.0	22.0	16.1
LAST	26.6	20.5	20.9	20.5	14.8
<i>8B models</i>					
Base-8B	71.2	45.8	43.4	44.4	32.0
LoRA-8B	57.1	42.3	36.0	34.8	25.5
ParMLP-8B	61.7	39.6	30.5	33.3	24.0
L-8TH-8B	69.1	39.7	35.1	36.0	24.8

B.2 Detailed InjecAgent Results

Table 7: Detailed InjecAgent results for 8B models. All values are percentages (%). **Valid Rate** is when model does successful tool calls.

Model	Valid Rate \uparrow	ASR (Total) \downarrow	Direct Harm \downarrow	Stage 1 \downarrow	Stage 2 \downarrow	Data Steal \downarrow
Base Attacks						
Base	42.3	70.6	73.4	75.6	92.7	68.3
LoRA	63.6	76.9	80.1	74.8	98.8	73.7
ParallelMLP	39.6	60.7	68.0	67.7	84.3	55.4
CALYREX (LATE8TH)	41.6	75.8	83.2	81.2	87.0	69.7
Enhanced Attacks						
Base	48.7	93.4	90.9	98.7	97.3	95.8
LoRA	77.2	92.6	94.5	91.1	100.0	91.0
ParallelMLP	61.6	82.4	91.7	89.6	83.9	74.5
CALYREX (LATE8TH)	59.9	88.0	90.2	95.3	90.3	85.8

B.3 1.5B Models Benchmarks Scores

Table 8: Benchmark results (%) for all 1.5B models. \downarrow = lower is better (attack success rate).

Model	MMLU	GSM8K	IFEval	Long-IFEval	SysBench	SQuAD	Glaive FC	IH-Chall.	InjecAgent \downarrow	MSJ \downarrow	TensorTrust \downarrow
Base	60.2	62.2	25.1	19.6	31.5	39.4	5.3	15.6	30.3	34.4	3.5
LoRA	57.8	50.3	24.4	15.8	23.4	19.8	17.7	19.6	73.6	79.7	2.9
ParallelMLP	59.9	59.7	31.2	20.6	25.4	43.8	13.9	17.8	27.1	45.6	2.6
ALL	60.2	58.2	20.9	10.8	24.6	22.1	18.1	20.3	81.9	92.5	3.4
EVERY2	60.2	60.5	24.6	12.0	24.6	28.5	19.0	19.9	57.6	89.7	3.2
LATEHALF	60.3	59.1	27.5	15.7	26.0	37.9	20.8	15.7	72.0	87.8	3.0
LATEHALF2	60.3	61.0	28.1	14.7	27.0	37.2	20.0	13.8	50.7	91.1	3.1
LATETHIRD	60.3	59.9	29.4	16.5	25.7	39.0	19.3	15.3	33.8	79.2	3.1
LATEQUARTER	60.3	59.4	30.7	19.5	27.4	40.5	16.5	17.5	32.0	61.1	2.9
LATE8TH	60.2	59.4	29.0	19.6	28.9	42.9	15.0	18.0	19.4	45.3	2.5
LAST	60.2	60.7	26.6	19.2	27.9	43.3	17.7	19.7	21.4	48.6	2.8

B.4 CAL Magnitudes

Table 9: CAL/Attn activation magnitude ratio (%) by config and layer.

Layer	ALL	EVERY2	LATEHALF	LATEHALF2	LATETHIRD	LATEQUARTER	LATE8TH	LAST	ParallelMLP
1	12.1	-	-	-	-	-	-	-	-
2	1.3	1.9	-	-	-	-	-	-	-
3	0.7	-	-	-	-	-	-	-	-
4	0.6	0.9	-	-	-	-	-	-	-
5	0.6	-	-	-	-	-	-	-	-
6	0.5	0.8	-	-	-	-	-	-	-
7	0.5	-	-	-	-	-	-	-	-
8	0.5	0.7	-	-	-	-	-	-	-
9	0.5	-	-	-	-	-	-	-	-
10	0.6	0.7	-	-	-	-	-	-	-
11	0.5	-	-	-	-	-	-	-	-
12	0.6	0.7	-	-	-	-	-	-	-
13	0.5	-	-	-	-	-	-	-	-
14	0.5	0.7	1.8	1.9	-	-	-	-	-
15	0.5	-	0.7	-	-	-	-	-	-
16	0.6	0.9	0.7	1.1	-	-	-	-	-
17	0.7	-	0.7	-	-	-	-	-	-
18	0.7	1.1	0.7	1.3	2.4	-	-	-	-
19	0.7	-	0.7	-	1.1	-	-	-	-
20	0.7	1.1	0.7	1.2	1.0	-	-	-	-
21	0.9	-	0.9	-	1.1	3.1	-	-	-
22	0.9	1.5	0.8	1.6	1.0	1.7	-	-	-
23	0.9	-	0.9	-	0.9	1.3	-	-	-
24	0.9	1.5	0.8	1.5	0.9	1.2	4.6	-	4.8
25	0.8	-	0.8	-	0.9	1.1	2.7	-	3.1
26	0.9	1.6	0.8	1.5	0.9	1.2	2.3	-	3.0
27	1.6	-	1.6	-	1.8	2.0	3.9	-	5.7
28	1.4	2.2	1.5	2.3	1.6	2.0	3.3	48.8	4.6